

Projection of rural and urban human thermal comfort in The Netherlands for 2050

R. E. Molenaar, B. G. Heusinkveld and G. J. Steeneveld

Meteorology and Air Quality Section, Wageningen University, The Netherlands

ABSTRACT: Hot summer days may lead to reduced thermal discomfort, labour productivity, and higher morbidity and mortality for vulnerable groups. The projected climate change may raise this thermal discomfort in the future. To implement measures to prevent adverse health conditions, robust estimates of the future human thermal comfort (HTC) are required. This study analyses the future HTC for both coastal and inland Dutch cities and countryside. The future conditions are based on the KNMI-06 climate scenarios. Using these scenarios, observed weather data from 1976 to 2005 are transformed to future weather design data representative for 2050. Subsequently, HTC expressed in the physiological equivalent temperature (PET) is estimated for these future scenarios. A substantial increase of heat stress abundance is foreseen in all climate scenarios, for both urban and rural areas, particularly, under the most intense warming. In these scenarios, the frequency of hours with heat stress will more than double, and the increase will develop faster in an urban canyon than in rural areas. In urban areas, PET shows a maximum as function of sky-view factor (SVF), i.e. for a smaller SVF a wind speed reduction increases the PET on one hand and shading reduces the PET on the other hand.

KEY WORDS climate change; human thermal comfort; heat stress; physiological equivalent temperature; climate scenarios; The Netherlands

Received 2 October 2014; Revised 18 June 2015; Accepted 21 June 2015

1. Introduction

Heat stress is a leading cause of weather-related human mortality and morbidity (Luber and McGeehin, 2008) and reduced labour productivity (Dunne *et al.*, 2013; Altinsoy and Yildirim, 2015). As temperatures are projected to increase due to climate change, the human thermal comfort (HTC) is expected to worsen. In The Netherlands, the excess mortality can rise to 12% during heat waves corresponding to about 30 additional deaths per day and per Kelvin above the climatological mean temperature (Huynen *et al.*, 2001). Here, we quantify the current and future HTC in The Netherlands.

The Netherlands is a small and densely populated country in northwest Europe, which has prevailing south-westerly winds and a maritime climate due to the proximity of the North Sea (class Cfb in the Köppen climate classification; Sluijter *et al.*, 2011; Figure 1). The population amounts to 16.8 million people, i.e. a population density of 488 inhabitants km⁻² (Centraal Bureau voor de Statistiek, CBS, 2014). More than 40% of the Dutch population lives in the Randstad area, i.e. the agglomeration of the cities of Amsterdam, Rotterdam, Den Haag, and Utrecht. The provinces making up the Randstad area cover 20% of the Dutch land surface, while it hosts 44% of the Dutch population, which comes



down to >1000 inhabitants km⁻² with even 1180 inhabitants km⁻² in the province of Zuid-Holland (Nijmeijer, 2000).

Climate scenarios developed by the Dutch national meteorological service project that the mean 2-m temperature will increase and that heat waves will become more frequent (van den Hurk *et al.*, 2006). This development will affect both the rural and urban HTC, but quantitative HTC projections are scarce despite earlier research efforts (Steeneveld *et al.*, 2011; Wolters and Brandsma, 2012; Heusinkveld *et al.*, 2014; Theeuwes *et al.*, 2014; Taleghani *et al.*, 2015). In addition, public awareness and institutional infrastructure to cope with adverse HTC is minimal in The Netherlands. To propose adequate measures to prevent adverse health for vulnerable groups (Uejio *et al.*, 2011), the future HTC requires quantification. Therefore, a quantitative assessment based on the human energy balance (Mayer and Höppe, 1987; Matzarakis *et al.*, 1999) is essential for urban planners to identify uncomfortable street canyons and for formulation of suitable countermeasures.

In general, previous HTC assessments have mostly been directly based on global or regional climate models (RCMs; Delworth *et al.*, 1999; Diffenbaugh *et al.*, 2007; Fischer and Schär, 2010; Sherwood and Huber, 2010; Willett and Sherwood, 2012). Their results originate from ensemble simulations with a single climate model. Results for their rather coarse grid cells may overlook local conditions. Also, these results provide limited temporal

* Correspondence to: G. J. Steeneveld, Meteorology and Air Quality Section, Wageningen University, PO Box 47, 6700 AA Wageningen, The Netherlands. E-mail: Gert-Jan.Steeneveld@wur.nl

The Netherlands

Area: 41,543 km²
 Population: 16,819,595 
 Population density: 405.1/km²
 Climate: Maritime Cfb
 Predominant wind direction: Southwesterly 

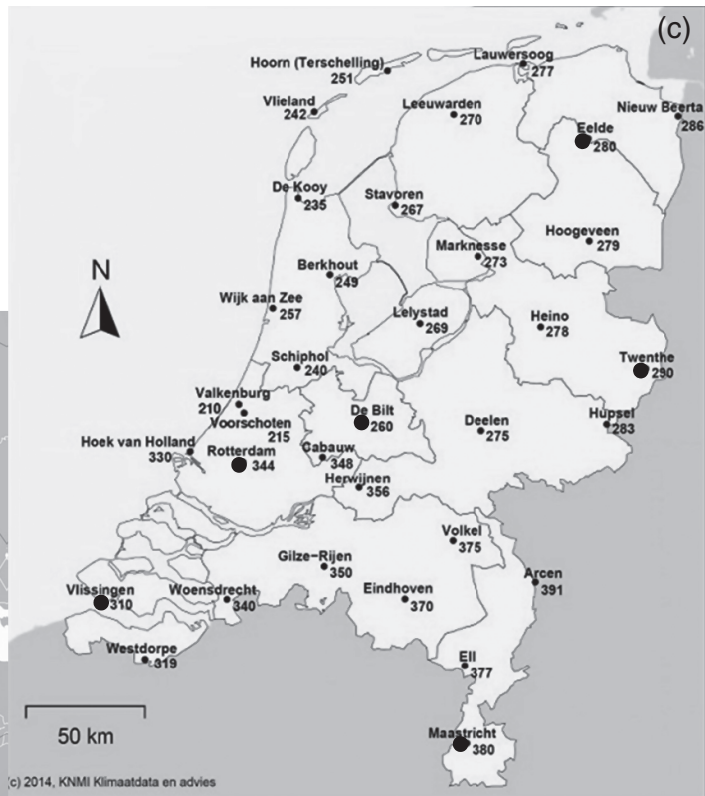


Figure 1. General information about The Netherlands (a) location of The Netherlands within Europe, (b) network of routine weather stations in The Netherlands, and (c) stations for which data are analysed in this study are indicated by large black dots. Note the number associated to a weather station refers to the WMO code of the station.

resolution (Matzarakis and Amelung, 2008), i.e. daily mean values. Therefore, we follow an alternative approach here in which climate model output is first translated into climate scenarios, which are subsequently applied to project current day meteorological time series future time series.

We quantify the Dutch HTC development by transforming current day meteorological time series to time series representing the year 2050 for four climate scenarios (Section 3.3). Subsequently, the trends in HTC are evaluated for six contrasting coastal and inland rural weather stations, including the effect of wind speed and radiation, and the analysis is based on hourly data. We quantify the human comfort trends within the urban environment.

The article is organized as follows. The next section briefly summarizes the physical background behind the relevant urban atmospheric physics and the human energy balance. Section 3 presents the methodology concerning the selected climate scenarios, data transformation, HTC calculation, and relevant site descriptions. The results and discussion are presented in Sections 4 and 5, respectively, whereas conclusions are drawn in Section 6.

2. Background: physics behind the urban heat island and thermal comfort

The urban climate differs from that of the rural surroundings. During daytime, solar radiation is absorbed

by the urban fabric due to a relatively low urban albedo. Moreover, long-wave radiation is trapped in the urban canyon due to the street canyon's limited sky view (Kusaka and Kimura, 2004; Theeuwes *et al.*, 2014). Also, anthropogenic energy consumption is a heat source for the urban environment. Furthermore, building materials have a relatively high heat capacity and conductivity, which dampens the amplitude of the diurnal air temperature cycle. Compared to rural surroundings, the city is sparse in vegetation, which reduces the evapotranspiration and thus the cooling. These physical processes causes the air temperature difference between city and countryside to be largest just after sunset (Oke, 1982).

Air temperature alone is insufficient to assess HTC, as it is also governed by the human body's net radiation, wind speed, humidity, as well as by human activity and clothing. Therefore, heat balance models of the human body that account for these aspects are powerful tools to analyse the HTC (Mayer and Höppe, 1987; Budd, 2001; Heusinkveld *et al.*, 2014). Here, we employ the heat balance model of the physiological equivalent temperature (PET), because it has a solid physical basis as a single thermal index to evaluate the thermal component of any given microclimate (Deb and Ramachandraiah, 2010). The PET is based on the Munich Energy-balance Model for individuals, which models the thermal conditions of the human body in a physiologically relevant way. PET is defined as the air temperature at which, in a typical indoor setting (without wind and solar radiation), the heat budget of the human body is

Table 1. Ranges of the physiological equivalent temperature (PET) for different grades of thermal perception by human beings and physiological stress on human beings internal heat production: 80 W, heat transfer resistance of clothing 0.9 clo (Matzarakis and Mayer, 1996).

PET (°C)	Thermal perception	Grade of physiological stress
<4	Very cold	Extreme cold stress
4–8	Cold	Strong cold stress
8–13	Cool	Moderate cold stress
13–18	Slightly cool	Slight cold stress
18–23	Comfortable	No thermal stress
23–29	Slightly warm	Slight heat stress
29–35	Warm	Moderate heat stress
35–41	Hot	Strong heat stress
>41	Very hot	Extreme heat stress

balanced with the same core and skin temperature as under the complex outdoor conditions to be assessed. As such, PET enables a layperson to compare the integral effects of complex thermal conditions outside with his or her own experience indoors. On hot summer days, for example, with direct solar irradiation, the PET value may be more than 20 K higher than the air temperature on a windy day in winter up to 15 K lower (Höppe, 1999; see Section 3.4).

This study uses the KNMI-06 scenarios to estimate the meteorological variable required for PET projections. In practice, PET estimates are performed by the RayMan model (Matzarakis *et al.*, 2000; Section 3.4), and classified according to HTC experience (Table 1). The defined classes indicate slight heat stress (PET: 23–29 °C), moderate heat stress (PET: 29–35 °C), strong heat stress (PET: 35–41 °C), and extreme heat stress (PET: 41 °C or higher).

To quantify HTC in urban areas, it is important to study streets that differ in orientation and aspect ratio. The sky-view factor (SVF) is commonly used to relate urban geometry and urban air temperature differences (Chen *et al.*, 2012). The higher the SVF, the more efficiently the urban canyon will receive solar radiation during daytime, but will also cool more rapidly in the evening (Kusaka and Kimura, 2004). Overall, in summer, the daytime short-wave shadow effects dominate over the long-wave trapping of radiation, while this is opposite in winter (Theeuwes *et al.*, 2014). Finally a small SVF reduces the urban canyon mean wind substantially.

3. Methodology

3.1. KNMI-06 climate scenarios

To transform current weather observations to future design weather data representing the year 2050, we use four scenarios as published by KNMI in 2006 (van den Hurk *et al.*, 2006). These scenarios have been formulated based on output for Western Europe from five global climate models to identify the large-scale steering parameters and from eight RCMs results for further regional refinement. The suite of RCM simulations used for the KNMI-06 scenarios was produced in the context of the European

PRUDENCE project (Christensen *et al.*, 2002), in which dynamical downscaling was applied using multiple RCMs and GCMs, all run for two 30-year episodes: a control period 1960–1990 and a future period 2070–2100, forced by two different Special Report on Emissions Scenarios (SRES) emission scenarios (A2 and B1). The change of the atmospheric variables between these two time slices has been estimated by a linear combination of the altered atmospheric circulation and a circulation independent contribution that reflects the direct response to a global temperature change (van den Hurk *et al.*, 2006). An extensive RCM evaluation for present day climate conditions was carried out, and analyses of the PRUDENCE RCMs highlighted unrealistic behaviour in precipitation and temperature for a minority of models. This gave rise to excluding one RCM, leaving eight RCM simulations nested in results from the HadAM3H atmosphere model (Jones *et al.*, 2001), and two RCMs driven by two different runs of the ECHAM4-coupled climate model. Hence, the RCM results have been grouped concerning their projected warming, circulation changes over Western Europe, and climate change in The Netherlands. These large-scale projections have been ‘translated’ to more detailed changes in temperature, precipitation, evaporation, and wind speed in The Netherlands.

Various climate model simulations provide considerably different changes in climate as a result of uncertainties in future greenhouse gas and aerosols emissions. Also, current scientific understanding of the physical processes in the climate system and their representation in climate models is limited (Teixeira *et al.*, 2008; Holtlag *et al.*, 2013). The uncertainty increases further when zooming in from a global scale to a regional scale, such as Western Europe or The Netherlands. Then, the uncertainty results from the variety of circulation patterns in the simulations. Many climate models show the possibility for a future change in circulation patterns above Western Europe, consisting of a reduced westerly circulation (van den Hurk *et al.*, 2006; Lenderink *et al.*, 2007). However, the magnitude and direction of this change differ between models. To account for these uncertainties, the KNMI-06 climate scenarios have been designed based on two criteria. One is temperature increase (global contribution) and the second is the atmospheric circulation change (regional contribution). The climate scenarios have not been based on emission scenarios, but simply to the increase in global mean temperature by 2050, i.e. either a moderate increase of +1 °C (labelled ‘G’) in 2050 relative to 1990, or a strong increase of +2 °C (labelled ‘W’) in 2050. For small-scale regions like The Netherlands, uncertainties are relatively large, particularly, due to atmospheric circulation. In general, a modified atmospheric circulation pattern in Western Europe significantly affects air temperature (van Ulden and van Oldenborgh, 2006). Thus, accounting for possible changes in circulation patterns is required. Therefore, two circulation regime changes are included in the scenarios, which are a strong circulation change (labelled ‘+’), which induces warmer and moister winter seasons and increases the likelihood of dry and warm

summertime situations and a weak change of circulation (not labelled). Overall, the four scenarios are G, G+, W, and W+ (Table 2). Current knowledge does not indicate which scenario is most probable.

From a practical point of view, these scenarios provide monthly change coefficients for selected meteorological variables for 2050 compared to 1976–2005. Future time series are constructed by using the four scenarios by transforming historic synoptic observations from 1976 to 2005 to the same period of time but representative for the year 2050. The produced time series represent average weather conditions for future climate scenarios, whilst preserving realistic weather sequences. Hence, the transformed series provides information about averages, variation between days, and the probability of extremes for a plausible climate in the future. A transformation tool has been developed to convert current day weather data to future design weather data for each scenario. The transformed time series do not provide a weather forecast in the future for specific days or a specific year (Bakker and Bessembinder, 2012, henceforth BB12).

3.2. Weather stations

Since the local climate varies between coastal and inland stations in The Netherlands, we have selected six approximately evenly spread weather stations for our analysis, i.e. De Bilt, Eelde, Rotterdam, Maastricht, Twente, and Vlissingen (Figure 1).

De Bilt (52°06'N, 05°11'E, +1.9 m above a.s.l.) is located in the centre of the country, east of Utrecht. Its observations have a high scientific value, because it has the longest homogenized Dutch record of historical data since 1901. Weather station De Bilt is also the country's main station for the general public. Observations in De Bilt are used to compose monthly and yearly evaluations, which are often adopted by the media. The observed wind speed at this station is relatively low compared to the other stations (see below). The weather station in De Bilt is substantially affected by nearby roughness elements as trees, parks and urban areas upwind of the prevailing wind direction (Wieringa and Rijkoort, 1983; Wever and Groen, 2009; Koopmans *et al.*, 2015). To obtain a more representative footprint for the wind observations, the measurement height of wind speed changed in 1993 from

10 to 20 m and its record is corrected to the 10-m level accounting for the surface roughness (Wever and Groen, 2009; De Jong and van Boxel, 2012). De Jong and van Boxel (2012), however, show that wind trends in De Bilt are inconsistent with wind trends in the more rurally located weather station Soesterberg (7 km northeast of De Bilt), and they question the representativeness of De Bilt as weather station for the inland wind climate.

The other stations are located at remote rural sites. Eelde (53°07'N, 06°35'E 3.23 m a.s.l.), is located in the northernmost station although relatively inland. The landscape is relatively open and flat with a sandy soil. Twente (52°16'N, 06°53'E, 33.02 m a.s.l.) is located on an army base weather station in the east of the country. The landscape is gently rolling with a mixture of forest and grassland on a sandy soil. Maastricht (50°54'N, 05°46'E, 112.72 m a.s.l.) is the most southerly located site of The Netherlands. This airport is located in gently rolling terrain with neighbouring grass and cropland. Several forested slopes are present in the surroundings. Rotterdam is a more coastal station and uses the weather station of airport Zestienhoven (51°58'N, 04°27'E, -5.43 m a.s.l.). This weather station is situated in a polder with grass land on a clay soil, with the city of Rotterdam nearby in the south. Vlissingen (51°27'N, 03°36'E, 8.04 m a.s.l.) is a coastal station positioned on the harbour pier of the Westerschelde, in the southwest of The Netherlands. In our analysis for rural terrain, we assume that the weather stations mentioned above do fulfil SVF = 1 and comprise local climate zone D (Stewart and Oke, 2012). As most stations are located in open terrain on airports, this assumption is reasonably justified.

3.3. Methodology transformation of time series

To construct design weather data representative for 2050 at hourly intervals, daily and hourly temperature, relative humidity (RH), wind velocity and cloud cover values for the reference period have been selected (KNMI, 2012; Figure 2). First, daily mean values of temperature and RH are transformed, resulting in daily change factors (X), which are subsequently applied to the hourly data of each day. Wind speed and cloud cover remain unchanged, because insufficient signal was obtained from RCM simulations for these variables (Bakker, 2013, personal communication; Lokys *et al.*, 2015). The procedure is as follows:

Table 2. Overview of KNMI-06 climate scenarios for The Netherlands.

Label	Character	Description
G	Moderate	1 °C temperature rise on earth in 2050 compared to 1990 no change in atmospheric circulation patterns in Western Europe
G+	Moderate+	1 °C temperature rise on earth in 2050 compared to 1990 + milder and more wet winters due to more westerly winds + warmer and drier summer due to more easterly winds
W	Warm	2 °C temperature rise on earth in 2050 compared to 1990 no change in atmospheric patterns in Western Europe
W+	Warm +	2 °C temperature rise on earth in 2050 compared to 1990 + milder and more wet winters due to more westerly winds + warmer and drier summer due to more easterly winds

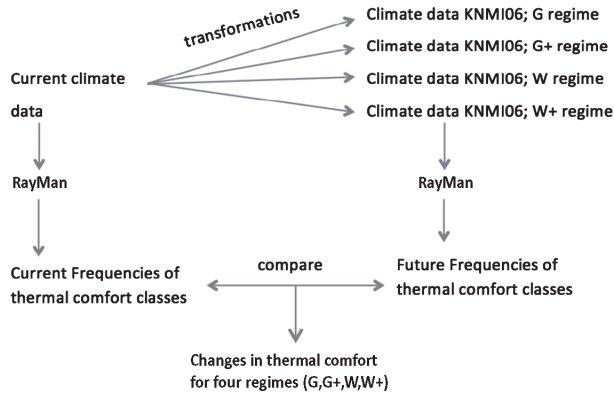


Figure 2. Workflow for estimating the human thermal comfort for the current climate and four future climate scenarios.

Step 1: Determination of the 10, 50, and 90 percentiles of the current-day temperatures: T_{10}^c , T_{50}^c , and T_{90}^c .

Step 2: For these percentiles, the temperature changes between 1990 and 2050 are applied, ΔT_{10} , ΔT_{50} , ΔT_{90} , respectively. These shifts are applied to the daily data, and have been tabulated by BB12, and are used here (Table 3).

Step 3: Determination of the 10, 50, and 90 percentiles of the future temperature T_{10}^f , T_{50}^f , and T_{90}^f :

$$T_{10}^f = T_{10}^c + \Delta T_{10} \tag{1a}$$

$$T_{50}^f = T_{50}^c + \Delta T_{50} \tag{1b}$$

$$T_{90}^f = T_{90}^c + \Delta T_{90} \tag{1c}$$

These temperature changes are applied to daily mean data.

Step 4: Estimation of the conversion factor α for daily mean data, defined as:

$$\alpha = \frac{(T_{90}^f - T_{50}^f)}{(T_{90}^c - T_{50}^c)}, \text{ if } T^c \geq T_{50}^c \tag{2a}$$

or,

$$\alpha = \frac{(T_{10}^f - T_{50}^f)}{(T_{10}^c - T_{50}^c)}, \text{ if } T^c < T_{50}^c \tag{2b}$$

Parameter α governs the change of the width of the temperature distribution and as such also the frequency of occurrence of warm days. This procedure implies that the changes for values higher than the 90th and lower than the 10th percentile are linearly extrapolated from the changes between the 50th and 90th or the changes between the 50th and 10th percentiles.

Step 5: Determination of the future daily mean data series (T^f):

$$T^f = T_{50}^f + \alpha (T^c - T_{50}^c) \tag{3}$$

Step 6: The conversion factor per day is obtained by

$$X = \frac{T^f}{T^c} \tag{4}$$

Step 7: Then, the transformed hourly temperature series is found by multiplying the original series by the just derived factor X

$$T^f_{\text{hourly}} = T^c_{\text{hourly}} \cdot X \tag{5}$$

In this procedure, T represents the temperature (K); c and f denote the current and future conditions, respectively.

For the transformation of RH (in %), we follow BB12. First, we determine the shift in the global radiation (ΔQ) as determined from the change in reference crop evapotranspiration (rate of evaporation for an extensive area of ≈ 0.10 m high green grass cover of uniform height, actively growing, completely shading the ground, and not short of water, ΔRCE , in %):

$$\text{Step 1: } \Delta Q = \max(0, \Delta RCE - 8\%) \tag{6}$$

ΔQ is calculated for each scenario per month by using Table 4. Subsequently,

$$\text{Step 2: } \Delta RH = -0.36 \cdot \Delta Q (\%) \tag{7}$$

Step 3:

$$RH^f = RH^c + \Delta RH \tag{8}$$

Step 4: Conversion factor per day:

$$X = \frac{RH^f}{RH^c} \tag{9}$$

Table 3. Temperature change in the 10th, 50th, and 90th percentile per calendar month of the average daily temperature in Celsius around 2050 compared to 1976–2005 (BB12).

Month	Temperature change in the 10th percentile				Temperature change in the 50th percentile				Temperature change in the 90th percentile			
	G	G+	W	W+	G	G+	W	W+	G	G+	W	W+
January	1.00	1.41	2.01	2.82	0.90	1.09	1.80	2.29	0.79	0.98	1.69	1.85
February	1.00	1.40	2.00	2.80	0.90	1.10	1.80	2.30	0.80	1.00	1.71	1.90
March	0.98	1.36	1.96	2.73	0.90	1.14	1.78	2.36	0.84	1.10	1.75	2.10
April	0.95	1.30	1.90	2.60	0.90	1.20	1.75	2.47	0.90	1.27	1.85	2.48
May	0.92	1.23	1.84	2.45	0.90	1.27	1.72	2.59	0.96	1.46	1.94	2.89
June	0.90	1.15	1.80	2.31	0.90	1.35	1.70	2.71	1.00	1.66	1.99	3.29
July	0.90	1.09	1.79	2.18	0.90	1.41	1.70	2.82	1.01	1.83	2.01	3.67
August	0.90	1.06	1.80	2.12	0.90	1.44	1.70	2.87	1.00	1.91	1.99	3.84
September	0.92	1.10	1.84	2.20	0.90	1.40	1.72	2.80	0.96	1.80	1.94	3.60
October	0.96	1.23	1.91	2.45	0.90	1.27	1.76	2.59	0.89	1.46	1.84	2.89
November	0.99	1.33	1.97	2.66	0.90	1.17	1.79	2.42	0.83	1.18	1.75	2.29
December	1.00	1.39	2.00	2.78	0.90	1.11	1.80	2.32	0.80	1.02	1.71	1.95

Table 4. Average monthly changes (%) in reference crop evapotranspiration around 2050 compared to the reference period 1976–2005 for the 4 KNMI-06 climate scenarios (BB12).

Month	G	G+	W	W+
January	1.4	1.3	2.8	2.6
February	1.5	1.5	3.1	3
March	1.8	2.2	3.7	4.5
April	2.5	3.6	4.9	7.1
May	3	5	6	10.1
June	3.4	6.5	6.7	13
July	3.5	7.8	7	15.7
August	3.4	8.5	6.7	16.9
September	3	7.6	6	15.2
October	2.4	5	4.7	10.1
November	1.8	2.9	3.6	5.8
December	1.5	1.7	3.1	3.4

Step 5:

$$RH^{\text{hourly}} = RH^{\text{hourly}} \cdot X \quad (10)$$

3.4. The RayMan model

We use the RayMan (v1.2, Matzarakis *et al.*, 2000) model to estimate the HTC for both rural and urban sites. In our study, RayMan uses time series of temperature, RH, wind speed and cloud cover at a rural station as input, and fish-eye photos of the street configuration. Herein, cloud cover is used to account for the attenuation of both short- and long-wave radiation. Initially, SVF=1.0 is used, to study the PET for the rural weather stations. For urban areas, a sky-view photo will be applied, so we account for the sun path that determines the incoming radiation during the year, and which depends on the day of the year and geographical coordinates. RayMan has been extensively validated for Northwest Europe in Matzarakis *et al.* (2007).

PET follows from a thermo-physiological heat balance model, which is the basis for the calculation of the physiologically equivalent temperature. PET is equivalent to the air temperature that is required to reproduce the energy exchange with a reference person's body in a reference environment as observed under the conditions being assessed. In detail, the model is based on the energy balance for the human body:

$$M + PW + R + C + E_D + E_{Re} + E_{Sw} + S = 0 \quad (11)$$

where, M the metabolic rate, PW the physical work output, R the body's net radiation, C the convective heat flux, E_D the latent heat flux to evaporate water diffusing through the skin, E_{Re} the sum of heat flows for heating and humidifying the inspired air, E_{Sw} the heat flow due to evaporation of sweat, and S the heat storage heat in the body mass. The reference environment has a water vapour pressure of 12 hPa, an RH = 50%, and a temperature of 20 °C. The assessment is made for a standard 35-year-old male, 1.75 m tall, weighing 75 kg, and who wears clothes with an insulation 0.9 clo (note 1 clo represents a heat resistance of 0.155 m² K W⁻¹) and has a metabolism of 80 W.

The RayMan model enables the user to predict thermal quantities of the body, i.e. skin temperature, core temperature, and sweat rate or skin wetness. The current analysis does not distinguish between men and women, because we expect the projected trends to be approximately similar. In practise, in the limit of no wind, RayMan is technically unable to estimate the HTC. Therefore, input wind velocities of 0 ms⁻¹ have replaced by 0.1 ms⁻¹. For the summer season, this correction has been applied to 1% of the input data. In addition, missing cloud cover, i.e. reported as '9 octa', has been replaced by $N=8$ octa, by assuming that most of the obstructed sky was due to very low clouds or fog (KNMI, 2005). This correction was performed for <1% of all the data in summer and over the year. As such, we assume that these corrections do not significantly influence the statistical results and conclusions of our study.

3.5. Sky-view factor

We estimate the SVF of three fish-eye photos for three contrasting urban environments, using a digital single-lens reflex camera Canon (Japan), type: EOS350D/Rebel XT (APS-c, 8 megapixel), with a circular fisheye lens by Sigma (Japan), with a focal length of 4.5 mm (type '4.5 mm F2.8 EX DC HSM' (Figure 3), and as such we cover a representative range of street configurations present in Dutch cities. We distinguish between the following locations:

- A relatively open area with high SVF of 0.84 in the 2e Rosestraat 9, Rotterdam, The Netherlands (51°54'0.07"N, 4°30'37.40"E, Figure 3(a)). This neighbourhood was classified as local climate zone 9 (sparsely built).
- A central business district located at Wilhelminaplein 50, Rotterdam, The Netherlands (51°54'28.74"N, 4°29'35.28"E, Figure 3(b)). This site has a SVF = 0.41, and has been classified as local climate zone 4 (open high rise).
- An east–west (E-W) street in a residential area located at Gouverneestraat 273, Rotterdam, The Netherlands (51°54'59.55"N, 4°28'10.29"E, Figure 3(c)), with a SVF = 0.26, and which was classified as local climate zone 3 (compact low rise).
- A north–south (N-S) street in a residential area located at Gouverneestraat 273, Rotterdam, The Netherlands (51°54'59.55"N, 4°28'10.29"E, Figure 3(d)), with a SVF = 0.26, and which was classified as local climate zone 3 (compact low rise).
- A residential area with trees located at Groen van Prinsterstraat, Wageningen, The Netherlands (51°57'45.16"N, 5°39'3.25"E, Figure 3(e)), with a SVF = 0.26, and which was classified as local climate zone 3 (compact low rise).

Sky-view photos have been taken in the middle of the selected street. SVF was estimated manually by identifying a polygon encompassing the sky in the photos, and RayMan has estimated the percentage of visible sky. For these particular sky-view photos, the SVF = 0.84

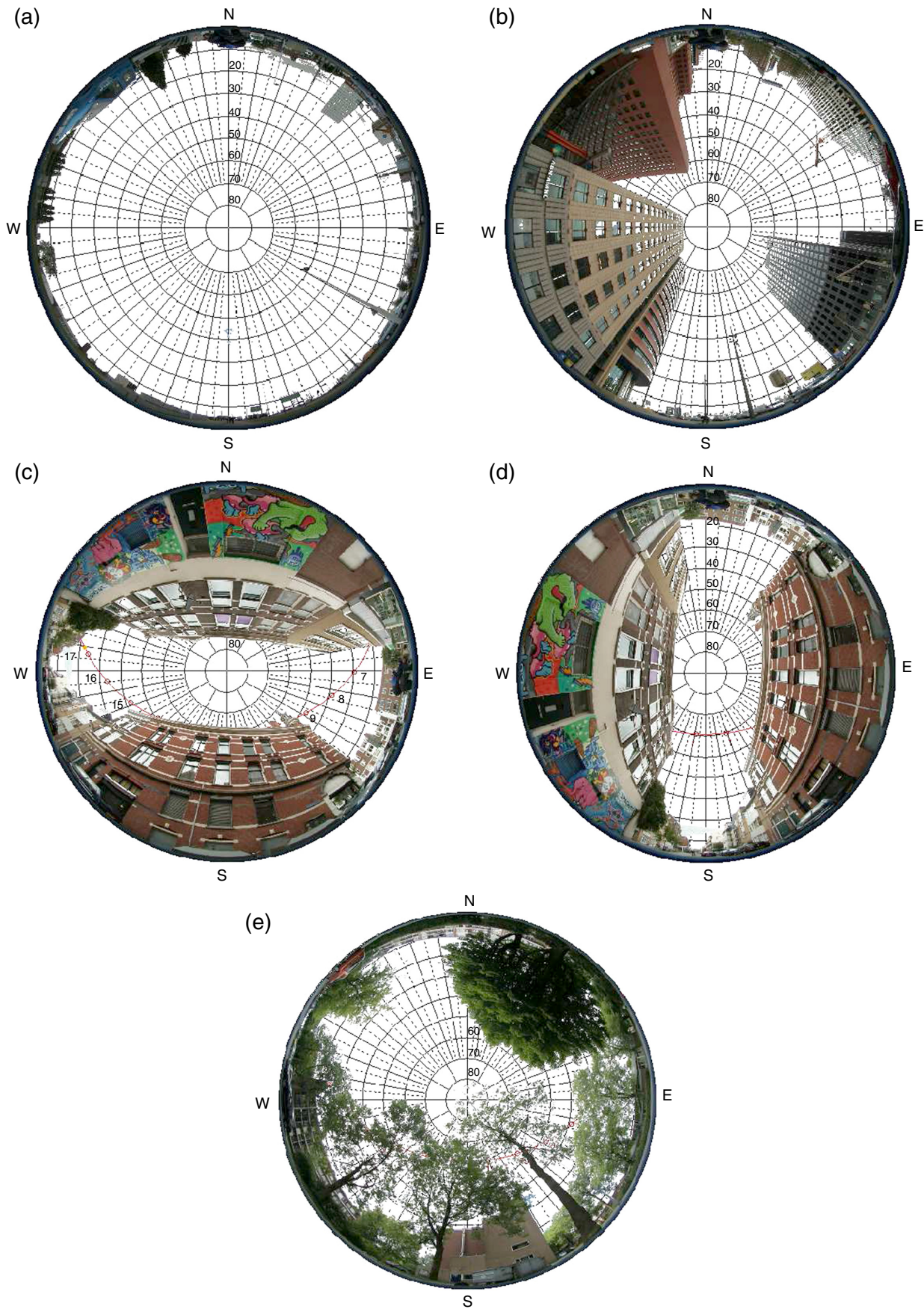


Figure 3. Sky-view photos for four sites with contrasting SVF (see text for details). (a) $SVF=0.84$, (b) $SVF=0.41$, (c) $SVF=0.26$ with east–west-oriented street and sun path (red line) for 3 July, (d) $SVF=0.26$ with north–south-oriented street and sun path (red line) for 3 July, and (e) $SVF=0.26$ and trees and sun path (red line) for 3 July.

(Figure 3(a)); SVF=0.41 (Figure 3(b)); SVF=0.26 (Figure 3(c)–(e)). Using the latter, we can study the impact of street orientation on PET for a constrained SVF, and distinguish between obstruction by buildings and by trees. To assess the representativeness of the selected sky-view photos, we note that Heusinkveld *et al.* (2014) about 2000 sky-view photos have been made for two bike traverses through Rotterdam of ≈ 10 km each. The mean SVF along these traverses (excluding the rural areas and dike areas) amounts to 0.42, with a standard deviation of 0.14, and a 5 percentile of 0.26 and 95 percentile of 0.64.

For the estimates of urban PET trends, these SVFs have been applied to all weather station data across the country. Hence, we assume that the impact of differences in architecture across the country is smaller than the impact of differences in rural climate.

3.6. Wind reduction

Wind speed substantially affects HTC and in fact is the second most important factor after shading (Mayer and Höppe, 1987; Andreou, 2013). In general, wind speeds in urban areas are reduced compared to surrounding rural areas (Johansson, 2012). When air flows from a rural area to an urban area, the atmospheric boundary layer adapts to the local building density. Consequently, the wind speed decreases due to increased roughness caused by physical obstacles (Fikirté and Yemer, 2010). RayMan has been developed to assess HTC, and the model accounts for the impact of street geometry to estimate radiative fluxes. However, the model does not translate the wind speed as measured in the countryside to values representative for the city, based on urban morphological characteristics or canyon characteristics as provided in the sky-view photo. This is a substantial deficiency for estimating HTC. Therefore, in this study, the wind speed that acts as input time series for RayMan has been reduced depending on the SVF and building height.

To quantify the wind speed reduction from the observed rural 10-m wind speed to the wind speed in the street canyon, we follow Oke (1988), who used the aspect ratio (building height H divided by street width W) of street canyons to categorize the flow. The wind reduction was estimated from a network of weather stations in Rotterdam (Heusinkveld *et al.*, 2014). For each urban station, the measured SVF was used to estimate the aspect ratio H/W (Oke, 1981), and subsequently, an empirical relation for the wind adjustment factor (WAF) was determined for height z (1.2 m in this study) above the ground is estimated by

$$\text{WAF} = e^{-\frac{H}{20W}} \quad (12)$$

Equation (12) is only valid for conditions for which it has been derived ($10 < H < 40$ m; $10 < W < 50$ m; $0.55 < \text{SVF} < 0.78$). As an illustration, consider a site typical Dutch building morphology of $H = W = 10$ m, and thus $\text{SVF} = 0.45$, which leads to $H/W = 1.0$ (Table 5). Then, $z/H \approx 0.12$, we find $\text{WAF} = 0.66$ and a wind speed reduction of 34% compared to the rural 10-m wind. Wind

Table 5. Relation between sky-view factor (SVF) and H/W (Oke, 1981).

H/W	Rural	0.25	0.5	1	2	3	4
SVF	1.00	0.89	0.71	0.45	0.24	0.16	0.12

direction dependence and secondary circulations in street canyons are not taken into account (Santiago *et al.*, 2007). Considering the uncertainties in the climate scenarios itself, and since the wind speed in the canyon is not the only ingredient for the PET estimation, we assume that excluding the wind direction effect does not add essential uncertainty. Wind speed is in fact the second most important factor for HTC (Andreou, 2013). For the sky-view photos in Figure 3(a) and (b), WAF amounts to 0.9 and 0.7 (following Table 5 and Equation (1)), while in Figure 3(c)–(e) $\text{WAF} \approx 0.3$.

4. Results

4.1. Thermal comfort rural environment

This subsection presents the projected HTC for the countryside, i.e. for a $\text{SVF} = 1$ and $\text{WAF} = 1$, expressed as the yearly hours with heat stress ($\text{PET} > 23^\circ\text{C}$). Table 6 presents the PET distribution for a rural environment around Rotterdam. Most of the heat stress hours are found in the slight heat stress class of $23 < \text{PET} < 29^\circ\text{C}$, i.e. ~ 178 h per year. Compared to the current climate, in this class, the number of yearly heat stress hours will increase by about 31 h in the G scenario, by 96 h in the G+ scenario, by 68 h in the W scenario, and by 116 h in the W+ scenario. Also, the other heat stress classes show strong increases of adverse HTC abundance.

Considering the class of $\text{PET} > 41^\circ\text{C}$, this range is hardly reached in the current climate for a 30-year period, and on average thus results in a vanishing frequency per year. In the future climate projections, this class will be populated more often, i.e. with 2, 8, 4, and 14 h per year in the G, G+, W, and W+ scenarios, respectively (Table 6).

Figure 4 shows the distribution of PET classes that result in thermal stress, i.e. $\text{PET} > 23^\circ\text{C}$. Compared to absolute differences in Table 6, this figure shows the relative differences in PET for Rotterdam and the changes that are projected over the different PET classes. Obviously, the relative abundance of the slight heat stress class will decrease in the projected climate and particularly the $35 < \text{PET} < 41^\circ\text{C}$ will gain abundance. This underlines that both the magnitude and frequency of the heat stress will increase in The Netherlands.

The bottom row in Table 6 aggregates the frequencies in the slight to extreme heat stress classes. The yearly average number of heat stress hours amounts to 262 in the current climate; 325 for the G scenario, 459 for G+ scenario, 398 for W scenario, and 510 h for the W+ scenario. Hence, under all scenarios, a substantial increase of heat stress, also in the countryside, is expected (see also next section). Under the W+ scenario, the amount of heat stress hours is

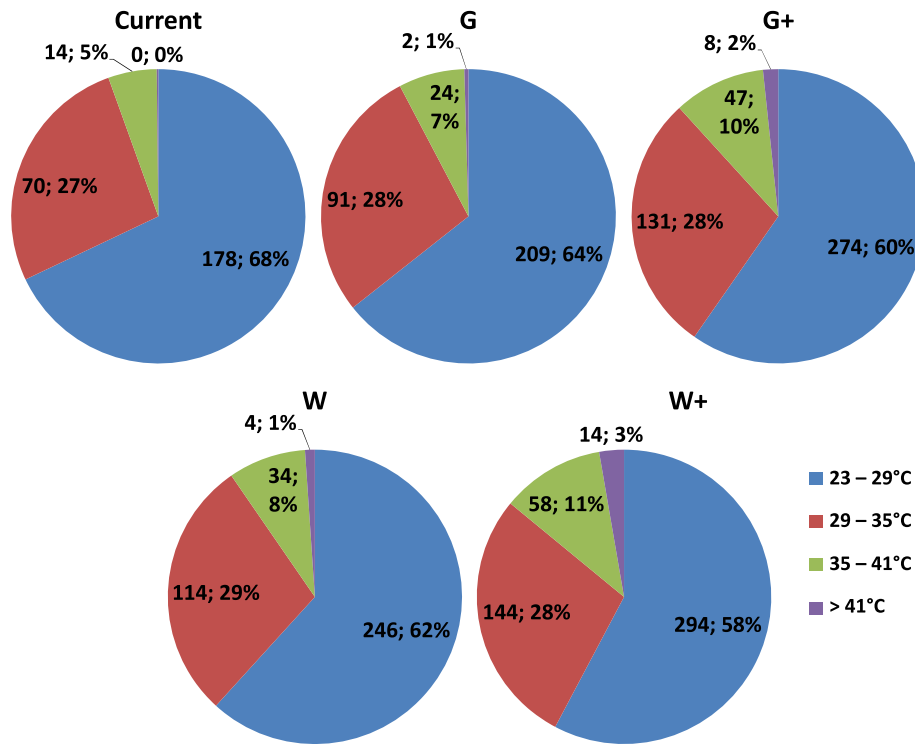


Figure 4. Distribution of current and projected (year 2050) yearly amount of hours with heat stress (PET > 23 °C) for the G, G+, W, and W+ climate scenarios for the city of Rotterdam. Notation: #hours per year; percentage of hours with heat stress.

Table 6. Number hours per year in each PET class in Rotterdam, averaged over 30 years. Current climate covers the reference period 1976–2005, for a rural climate (SVF = 1.00) for Rotterdam.

PET	Current	G	G+	W	W+
<4 °C	4215	3832	3662	3417	3121
4–8 °C	1488	1504	1359	1559	1553
8–13 °C	1577	1680	1577	1747	1729
13–18 °C	863	1001	1167	1146	1265
18–23 °C	362	425	543	499	588
23–29 °C	178	209	274	246	294
29–35 °C	70	91	131	114	144
35–41 °C	14	24	47	34	58
>41 °C	0	2	8	4	14
Sum PET >23 °C	262	325	459	398	510

almost double of the current amount of heat stress hours in Rotterdam. Values in the last row of Table 6 can slightly differ from the sum of the individual rows due to round off errors. Our findings compare reasonably well with results in Lokys *et al.* (2015) for northern Luxemburg (see Section 5).

It is interesting to study the difference in the temperature and the PET development. Figure 5 shows that for the rural area around Rotterdam, the mean change in PET is higher than for the air temperature itself. This difference increases with the intensity of the projected climate change, i.e. in the G scenario the difference amounts to 0.1 °C, while it amounts to 0.3 °C in the W+ scenario. Analogous results were found for the other weather stations (not shown). These results confirm findings by Oleson *et al.* (2015), who found that urban heat stress increase exceeds the temperature increase, based on a modelling

study for the United States for the period 2046–2065. They report that the heat stress increase is 0.5–1.0 °C higher than for temperature depending on urban density class and heat index (in their case Heat Index, Apparent Temperature, and Humidex). In our study, the excess PET increase amounts to 0.1–0.4 °C.

Figure 6 depicts the frequency of the HTC for all cities for the different PET classes and the different KNMI-06 scenarios. Figure 6(a) shows the results of PET class 23–29 °C. It appears that the stations that are located relatively inland, i.e. Maastricht, Twente, and De Bilt have the highest amount of heat stress for this class in the current climate, with about 220 h per year. The lowest heat stress abundance is found in Eelde, Rotterdam, and Vlissingen, with about 170, 180, and 130 h per year, respectively. The latter will rise to 243 h per year in the W+ scenario, i.e. about a doubling and an increase of 111 h. Under that

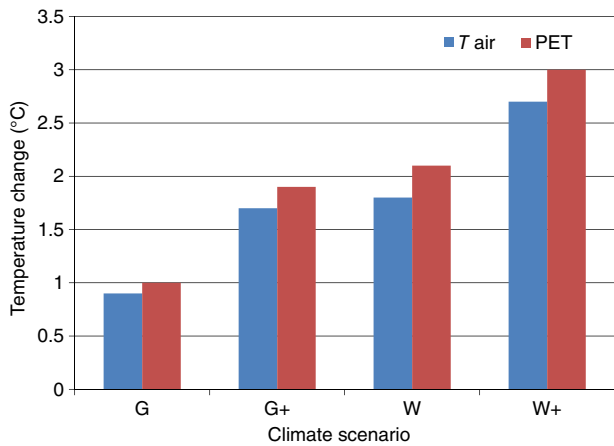


Figure 5. Mean air temperature and PET change for Rotterdam for the studied climate scenarios.

extreme scenario, Vlissingen will experience a similar dose of heat stress as the station with the most stress under the current climate, i.e. Maastricht.

The highest frequency of heat stress for the $23 < PET < 29^{\circ}\text{C}$ class is found in the G+ and W+ scenario (Figure 6). Both in the current climate and in the G scenario, Maastricht contains the highest amount of heat stress with 235 and 269 h per year, respectively. In the other scenarios (G+, W, and W+) the peak location moves

to De Bilt. For example, the frequency increases from 225 h per year in the current climate to 335 h per year in the G+ scenario, which is an increase of almost 50% with an extra of 110 h per year. In the W+ scenarios, this is even more and reaches 356 h, an increase of 131 h per year.

With respect to the other sites, an analogous increase of heat stress is found. The average number of heat stress hours amounts to almost 200 h in the current climate in this PET class. In the G+ and W+ scenario, this rises to on average > 300 h per year.

Regarding the moderate heat stress class, Figure 6(b) shows the number of heat stress hours for PET class $29-35^{\circ}\text{C}$. An analogous pattern as for the previous class is found, i.e. the coastal stations (Vlissingen, Eelde, and Rotterdam) experience the lowest heat stress load. Vlissingen counts for the current climate 45 h in this class, although this is projected to increase to 104 h in the G+ scenario and 112 h in the W+ scenario, which is more than a doubling. In general, results for other cities confirm this finding in this class. The highest frequency is found again in the G+ and W+ scenario as in Figure 6(a). Also, it is remarkable that De Bilt, Rotterdam, and Vlissingen contain more heat stress hours under the G+ than under the W scenario. Surprisingly, the ΔT_{90} for both classes is approximately equal for the months July, August, and September. However, for these months the G+ climate scenario has a somewhat larger increase in reference crop evapotranspiration than

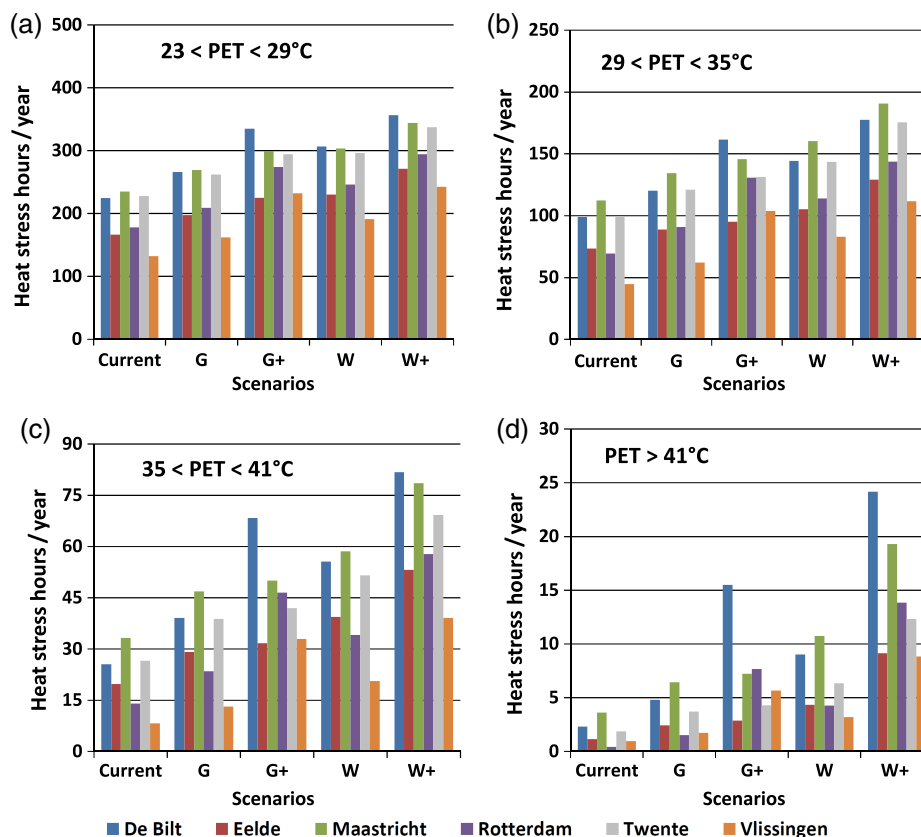


Figure 6. Number of heat stress hours per year for the weather stations De Bilt, Eelde, Maastricht, Rotterdam, Twente, and Vlissingen for the different KNMI-06 scenarios for rural environment ($SVF = 1.00$). (a) Slight heat stress PET class $23-29^{\circ}\text{C}$, (b) heat stress PET class $29-35^{\circ}\text{C}$, (c) strong heat stress $35-41^{\circ}\text{C}$, and (d) extreme heat stress class $PET > 41^{\circ}\text{C}$.

under the W scenario (see Table 4). As a result, the RH increase is stronger under the G+ scenario than under the W scenario (see Equation (7)). The higher PET frequency in this class for the G+ scenario is thus due to the humidity contribution to the HTC. The time series for Eelde, Maastricht, and Twente do not show this counterintuitive behaviour, probably, because of the contrasting RH regime because these stations are more inland than the three former stations. Thus in Equation (6), these latter stations are in a different regime than under the W+ scenario, i.e. a RH change in the G+ scenario but a near zero change in the W scenario. Hence, for these stations the amount of heat stress hours is higher for the W scenario compared to the G+ scenario.

Figure 6(c) reveals the heat stress number in the PET class of 35–41 °C. Also here the G+ and W+ scenarios contain the highest amount of heat stress numbers. Remarkably, weather station De Bilt shows high peaks for these scenarios. Most likely, this is a result of an underestimation of the wind speed at this station, as explained in Section 2.3. The same behaviour for weather station De Bilt is found for the HTC in the most extreme heat class of PET > 41 °C (Figure 6(d)). These extreme thermal conditions occur especially on days with low cloud cover and low wind speed. Also for the other stations, a

relatively large increase of heat stress hours is projected. In the current climate, PET values higher than >41 °C hardly exists. The lowest frequency is found in Rotterdam with 1 h per year and the highest in Maastricht with 4 h per year. In the G scenario, this raises to 2 h in Rotterdam and 6 h in Maastricht. For the W+ scenario, this amounts to 14 for Rotterdam and 19 for Maastricht. Also, the other stations show a similar percentage increase. Lokys *et al.* (2015) presented analogous findings for Luxemburg with the absence of the extreme heat stress class at the moment and a projected abundance of 10 h per year in the far future.

4.2. Thermal comfort urban environment

4.2.1. Heat stress hours urban environment

Figure 7 shows the yearly number of hours with heat stress for the various KNMI-06 scenarios averaged the six weather stations for the different SVFs and PET classes. We use the sky-view photos taken in Rotterdam also for the other cities in The Netherlands. As the architecture does not differ substantially between different areas in the relatively small country, this assumption is not unreasonable.

The results for the relatively open area represented by Figures 3(a) and 7(a) are analogous to those discussed for the rural area in the previous section. In the current climate,

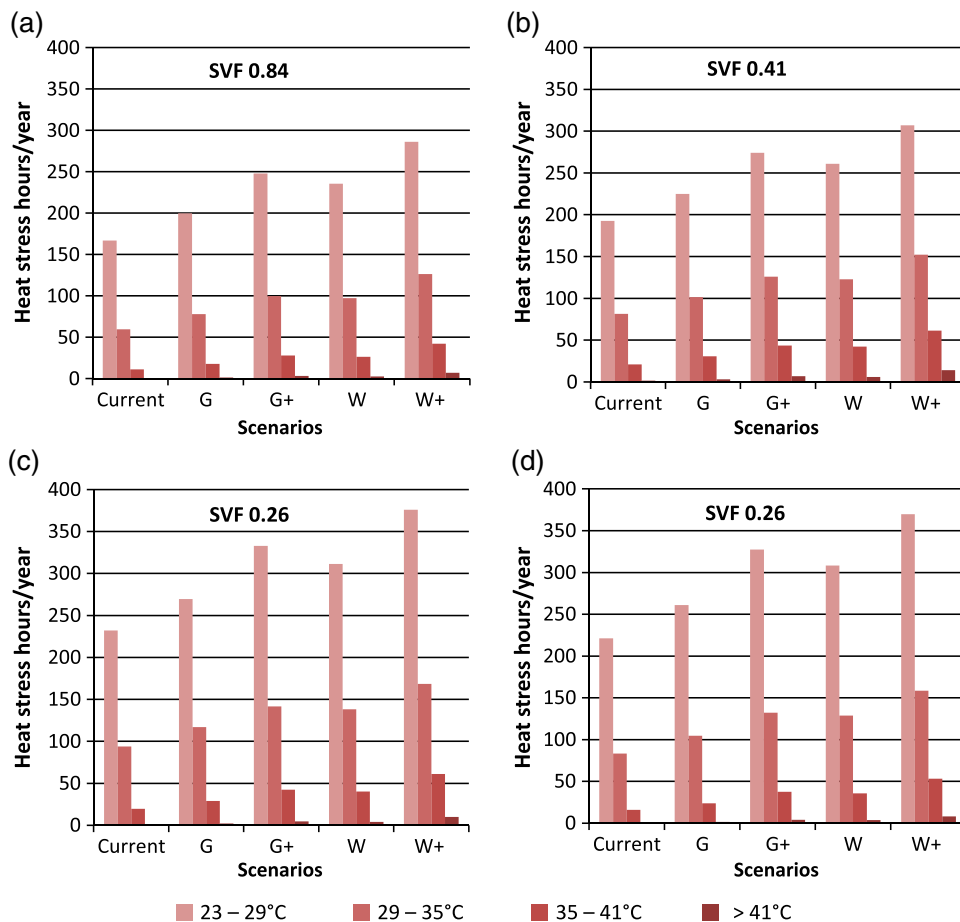


Figure 7. Number of heat stress hours per year for the current climate and the four climate scenarios, averaged over De Bilt, Eelde, Maastricht, Rotterdam, Twente, and Vlissingen for urban areas with different SVFs. (a) SVF=0.84, no trees; (b) SVF=0.41, no trees; (c) SVF=0.26, no trees; (d) SVF=0.26 and with trees.

the number of hours is about 220 h of heat stress (i.e. the sum of all heat stress classes), which increases to ~290 h in the G scenario, 380 h in the G+ scenario, 355 in the W scenario, and 455 h in the W+ scenario.

Figure 7(b) reveals that the amount of heat stress (PET > 23 °C) equals 296 h per year for the current climate, 361 h for the G scenario, 451 h for G+ scenario, 432 h for the W scenario, and 535 h per year for the W+ scenario. Compared to the current climate, this results in an increase of 22% for G, 52% for G+, 46% for W, and 80% for W+. An analogous development is projected for a street with SVF=0.41, with again the highest amount of heat stress occurs under the G+ and W+ scenarios (Figure 7(b)). Moreover, in the current climate, PET > 41 °C occurs only 2 h per year if we take the average for all the six stations. However, in the G, G+, W, and W+ scenarios, this will be respectively 3, 7, 6, and 14 h per year.

Figure 7(c) presents results for a representative example of an E-W-oriented urban canyon. This configuration shows also the highest amount of heat stress. The yearly amount of heat stress is 347 h in the current climate. In the climate projections, these values will raise to 417 for G, 522 for G+, 494 for W, and 615 for the W+ scenario. Compared to the current climate, this is an increase of respectively 70, 175, 147, and 268 h per year. This is approximately the same relative increase compared to the previously discussed configurations and for some scenarios even more. Compared to rural conditions, this increase is significantly higher. For example, if we take the sum of the total amount of heat stress in the rural climate SVF=1.0 (Figure 3), this will lead to 300 h in the current climate. In the KNMI-06 climate projections, this will be 366 for G, 458 for G+, 437 for W, and 541 for W+. Compared to the current climate, this is an increase of 66, 158, 137, and 241 h per year. These values of the rural climate projections are lower than those that are found for the urban climate. Hence, we conclude that the total amount of heat stress would develop fastest in urban areas.

Figure 7(c)–(d) shows the differences between an E-W street without trees and a street with trees. The amount of heat stress does not differ substantially between the N-S and an E-W street. Overall, the total amount is slightly lower in a street with trees. However, if we zoom in on the more extreme heat stress classes, the effect of the vegetation is more evident. For example, for PET > 41 °C for the W+ scenario, ten heat stress hours per year in an urban E-W street without trees are expected. In a street with trees, this is only 8 h per year. Hence, including trees in a street will lead to 20% less extreme heat stress hours in this climate projection. Considering the class of 35 < PET < 41 °C, the case without trees results in 61 heat stress hours, while this amounts to 53 h per year with trees, i.e. a decrease of 13%.

In general, Figure 7 shows that the wind speed reduction due to SVF results in an increase of the overall number of heat stress hours. However, for the most extreme conditions (PET > 41 °C), a different development is found. For example, in the W+ scenario, the number of hours with heat stress in class PET > 41 °C amounts to 14 h per year

with SVF=0.84 (Figure 7(a)), increases for SVF=0.41, and then decreases for the SVF=0.26 cases (Figure 7(c) and (d)). This can be explained by the mechanism as explained in Theeuwes *et al.* (2014). The street canyon radiation balance, and thereby also PET, is the net effect of trapping of long-wave radiation and by shadow effects to the short-wave radiation. For relatively large SVF, the long-wave radiative trapping effects dominate for a reduction of the SVF, i.e. short-wave radiation is still able to enter the canyon, although long-wave radiation is less efficiently able to leave the canyon, resulting in an increased temperature and PET. For very narrow canyons, also the solar radiation can limitedly enter the canyon, resulting in a cooling effect and hence less stress. In addition, narrow canyons result in a substantial wind speed reduction, which increases the PET for low SVF. Apparently, the last mechanism dominates for small SVFs in our analysis too.

4.2.2. Role of street orientation

Results for PET for N-S and E-W-oriented streets and with trees are presented in Figure 8 for a 24 h time interval. The red line indicates the sun path, which varies during the year. In summer, the sun path is relatively longer, which results in more solar radiation into the canyon. The plotted sun path in Figure 3(c)–(e) represents the path for 3 and 4 July 1976 (a warm summer period). Figure 8 shows the PET development for the three different street configurations. Streets that are oriented E-W are exposed to direct radiation than N-S-oriented streets, which may result in a larger radiation and PET dose. Differences are most prominent during daytime around noon, especially, the street with trees show lower PET values. For example, the maximum PET values found on 3 July are 47 °C for the N-S street, 44 °C for the E-W street, and 41 °C for a street with trees. Night-time PET values are identical for these days. Remarkable is that the N-S-oriented street has higher max of PET than for the E-W-oriented street. In this example, the E-W street contains more shadow around noon because the sun path is blocked (Figure 3(d)). This causes the higher peak in PET in the N-S-oriented street.

Figure 8 reveals that shading is an important factor in influencing the PET. This fact points out the necessity of shading as a main strategy for keeping the street area in a comfortable HTC range (Ali-Toudert and Mayer, 2006). N-S orientation experience a noticeably shorter period of time of discomfort than E-W streets. The N-S-oriented street does contain sometimes a higher peak of maximum PET. However, the highest dose of heat stress (PET > 23 °C multiplied by the number of hours in that class) is higher for E-W orientation. It is important to notice that the current approach with the selected sky-view photos only give heat stress estimates for the middle of the street. The finally experienced heat stress depends of course on the precise location in the street, because parts of the street might be shadowed while others are not, depending on the time of the day and the season (Ali-Toudert and Mayer, 2006). Overall, a certain shading level depends on urban street configuration and thus on aspect ratio and

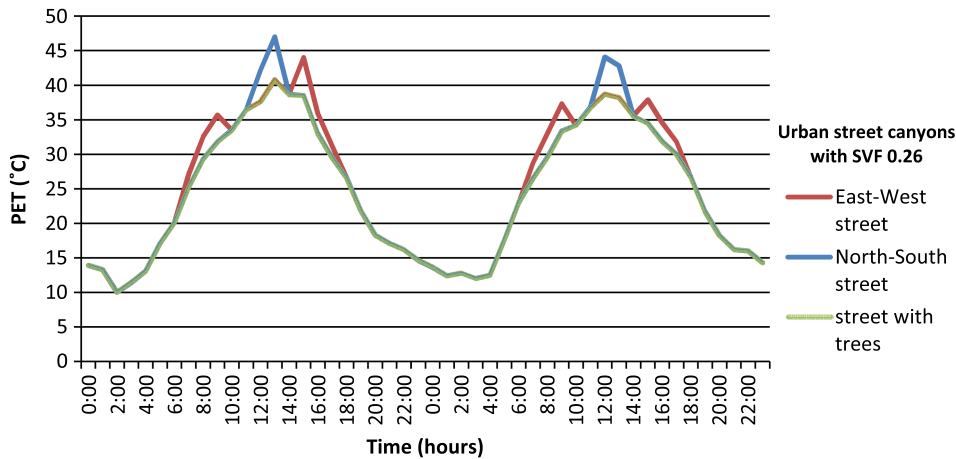


Figure 8. Diurnal evolution of PET on 3 and 4 July 1976 for streets with SVF = 0.26 but varying street orientation and presence of trees.

street orientation. Also, a good addition to create shade would be to plant trees to improve the original thermal environment in summer (Hwang *et al.*, 2011). This was confirmed in our results, where the street with trees experiences relatively low PET values.

5. Discussion

In this section, we compare our results with results from earlier studies in Europe, the consequences of the PET trends for society, and we reflect on the followed research strategy.

Lokys *et al.* (2015) studied PET projections for Luxemburg (~500 km southeast of The Netherlands), and they found that the class PET >41 °C is currently absent but will appear ~10 h year⁻¹ in 2050, which is a results close to our study. Similar results for Luxemburg were reported in Junk *et al.* (2014). In addition, the frequency of heat stress hours (PET > 23 °C) increased by a factor 2–4 for Luxemburg, while we found at maximum a doubling for the W+ scenario.

Thorsson *et al.* (2011) performed an analogous study for Goteborg (Sweden), and found that hours of strong/extreme heat stress are expected to triple between the period 1980–1999 and 2080–2099. In our study, the frequency of PET > 35 °C will increase by a factor 1.9, 4, 2.7, and 5 for the G, G+, W, and W+ scenarios, respectively. Furthermore, the number of hours with no thermal stress increases by 40–200 h year⁻¹ in Thorsson *et al.* (2011), whereas for our study, the number of hours that are ‘comfortable’ increases by 120 h from the current conditions to the W+ scenario. Overall, the raised PET values may lead to enhanced heat-related mortality (Astrom *et al.*, 2011).

Recently, Böcker and Thorsson (2014) studied the impact of HTC on the urban mobility in Rotterdam. In terms of transport modes, their study indicated an increased use of cars at the cost of bikes for PET > 23 °C. At the same time, the time spent cycling and the number of cycling trips per person per day decreased for PET > 23 °C.

Overall, our results indicate a strong PET increase and therefore, a change in mobility modes is expected. This may raise new demands in urban infrastructure for future conditions. In addition, the presented PET developments provide key information for application of climate tourism information schemes to assess possible changes in tourism potential in The Netherlands (Matzarakis *et al.*, 2013).

The substantial increase in frequency of high PET values in The Netherlands raises the question of most suitable methods to circumvent adverse HTC via interventions in urban planning. For Oberhausen (Germany, not far from the Dutch boarder), Müller *et al.* (2014) identified that increasing wind speed was the most effective adaptation measure. Also, it appeared that vegetation areas show greater PET reductions by the combined effect of shading and evapotranspiration than water surfaces alone. Hence, the construction of parks with sufficient water supply and tall, isolated, shade-providing trees that allow for adequate ventilation are recommended for planning.

The formulated climate scenarios that we use as the basis for the HTC projections contain some uncertainties. The transformed time series give information on averages, variation between days, the probability of extremes, etc. for a plausible climate in the future. The transformed time series do not predict either the future weather on a specific day or in a specific year (BB12). Moreover, climate projections also ignore for future city development, which affect HTC as well.

Also, we note that in the estimation of the urban PET, the UHI effect has not been applied because during heat stress hours (daytime), city temperature is only slightly raised compared to the countryside. Furthermore, it is rather uncertain to estimate the UHI effect for future conditions, because several studies report contrasting results concerning this trend (e.g. Wilby, 2003; Rosenzweig *et al.*, 2005; McCarthy *et al.*, 2010; Oleson *et al.*, 2011; Oleson, 2012).

This problem is even more prominent for UHI estimation on hourly basis in such long time records. A fixed UHI would result in an underestimated urban temperature in calm summer nights, but an overestimated urban temperature in windy conditions. A scaling of the UHI with

these atmospheric conditions is so far unavailable. Therefore, any correction for the UHI would induce spurious results and should be avoided. Hence, we omit any correction, but remark that our results should be considered as a lower boundary of the PET regimes in urban areas.

In our study, we analysed only a limited amount of sky-view photos. For a more complete picture of the HTC on a local scale, more of these sky-view photos have to be analysed, particularly, for a variety of vegetation configuration. However, the current samples provide data for a broad and relevant sample for contrasting sites and thus offer a wide spectrum of projected urban HTC development.

Finally, we note that KNMI recently published revised climate scenarios (KNMI, 2014). The new scenarios adopt the same strategy with four regimes, and their projections of the relevant meteorological variables for HTC differ only slightly from those for the KNMI-06 scenarios, and therefore our HTC projections are expected not to deviate much from the HTC projections with the new scenarios.

6. Conclusion

This study presents a projection of the future thermal comfort for The Netherlands, based on four climate scenarios as formulated by the Royal Netherlands Meteorological Institute. These scenarios distinguish between a moderate and warm regime, and regimes with and without future circulation changes. Observed weather data from 1976 to 2005 are transformed to future weather design data representative for the climate of 2050, and the PET is estimated for both coastal and inland rural weather stations, four contrasting urban street configurations, and four climate scenarios.

The amount of hours with heat stress will substantially increase in the future, under all scenarios, with most scenarios resulting in a doubling of the hours with heat stress ($PET > 23^{\circ}\text{C}$). The heat stress abundance will increase by 66, 158, 137, and 241 h per year for the G, G+, W, and W+ scenarios, respectively. In a typically Dutch urban environment, these intensifications amount to 70, 175, 147, and 268 h per year. Moreover, while the class of the most intense heat stress ($PET > 41^{\circ}\text{C}$) is currently absent, it will appear for 14 h per year in the W+ scenario by 2050. Overall, the most prominent HTC reductions are found in scenarios with a wind circulation change and relatively dry summers.

Street configurations largely affect the projected thermal comfort via reduced wind speed and shadowing. E-W-oriented streets experience less shadow during daytime than N-S-oriented streets, and thus a higher PET magnitude. On the contrary, streets with relatively high vegetation cover experiences a reduced PET. Especially, the abundance of the extreme PET-classes can be reduced by 20% by including trees in a street with the same sky view. Results show that the number of heat stress hours will increase for decreasing SVF. However, our projections indicate that for the most extreme warm weather, the city

is most comfortable during daytime, which is explained by the fact that streets provide more shadow compared to rural areas where the highest PET values are reached.

Overall, we conclude that thermal discomfort will substantially increase for all studied climate scenarios in The Netherlands. This new quantitative insight is useful in decision making for health, tourism, and regional planning purposes.

Acknowledgements

The authors acknowledge the NWO E-science project 'Summer in the City' (file number 027.012.103). We thank KNMI for providing routine weather station data and Alexander Bakker for advice on the transformation tool. We acknowledge Bert Holtslag for his valuable comments on the article.

References

- Ali-Toudert F, Mayer H. 2006. Numerical study on the effect of aspect ratio and orientation of an urban street canyon on outdoor thermal comfort in hot and dry climate. *Buill. Environ.* **41**: 94–108.
- Altinsoy H, Yildirim HA. 2015. Labor productivity losses over western Turkey in the twenty-first century as a result of alteration in WBGT. *Int. J. Biometeorol.* **59**: 463–471.
- Andreou E. 2013. Thermal comfort in outdoor spaces and urban canyon microclimate. *Renew. Energy* **55**: 182–188.
- Astrom DO, Forsberg B, Rocklov J. 2011. Heat wave impact on morbidity and mortality in the elderly population: a review of recent studies. *Maturitas* **69**: 99–105.
- Bakker A, Bessembinder J. 2012. Time series transformation tool description of the program to generate time series consistent with the KNMI '06 climate scenarios. Technical Report TR-326, KNMI, Rotterdam, The Netherlands, 75 pp.
- Böcker L, Thorsson S. 2014. Integrated weather effects on cycling shares, frequencies, and durations in Rotterdam, The Netherlands. *Weather Clim. Soc.* **6**: 468–481.
- Budd GM. 2001. Assessment of thermal stress-the essentials. *J. Therm. Biol.* **26**: 371–374.
- Centraal Bureau voor de Statistiek (CBS). 2014. *Population and population dynamics; month, quarter and year*. <http://statline.cbs.nl/StatWeb/publication/?VW=T&DM=SLEN&PA=37943eng&LA=EN> (accessed 10 January 2014).
- Chen L, Ng E, An X, Ren C, Lee M, Wang U, He Z. 2012. Sky view factor analysis of street canyons and its implications for daytime intra-urban air temperature differentials in high-rise, high-density urban areas of Hong Kong: a GIS-based simulation approach. *Int. J. Climatol.* **32**: 121–136.
- Christensen JH, Carter T, Giorgi F. 2002. PRUDENCE employs new methods to assess European climate change. *Eos* **83**: 147.
- Deb D, Ramachandraiah A. 2010. The significance of physiological equivalent temperature (PET) in outdoor thermal comfort studies. *Int. J. Eng. Sci. Technol.* **2**: 2825–2828.
- Delworth T, Mahlman J, Knutson T. 1999. Changes in heat index associated with CO_2 -induced global warming. *Clim. Change* **43**: 369–386.
- Diffenbaugh NS, Pal JS, Giorgi F, Gao X. 2007. Heat stress intensification in the Mediterranean climate change hotspot. *Geophys. Res. Lett.* **34**: L11706.
- Dunne JP, Stouffer RJ, John JG. 2013. Reductions in labour capacity from heat stress under climate warming. *Nat. Clim. Change* **3**: 563–566.
- Fikirté M, Yemer B. 2010. Urban wind map for Delft Rotterdam and Zoetermeer, Technische Universiteit Delft, Delft, The Netherlands, 93 pp. http://www.lr.tudelft.nl/fileadmin/Faculteit/LR/Organisatie/Afdelingen_en_Leerstoelen/Afdeling_AEWE/Wind_Energy/Education/Masters_Projects/Finished_Master_projects/doc/Fikirté_Yemer_r.pdf (accessed 21 July 2013).
- Fischer EM, Schär C. 2010. Consistent geographical patterns of changes in high-impact European heatwaves. *Nat. Geosci.* **3**: 398–403, doi: 10.1038/ngeo866.

- Heusinkveld BG, Steeneveld GJ, van Hove LWA, Jacobs CMJ, Holtslag AAM. 2014. Spatial variability of the Rotterdam urban heat island as influenced by urban land use. *J. Geophys. Res.* **119**: 677–692.
- Holtslag AAM, Svensson G, Baas P, Basu S, Beare B, Beljaars ACM, Bosveld FC, Cuxart J, Lindvall J, Steeneveld GJ, Tjernström M, van De Wiel BJH. 2013. Stable atmospheric boundary layers and diurnal cycles: challenges for weather and climate models. *Bull. Am. Meteorol. Soc.* **94**: 1691–1706.
- Höppe P. 1999. The physiological equivalent temperature – a universal index for the biometeorological assessment of the thermal environment. *Int. J. Biometeorol.* **43**: 71–75.
- Höppe P, Mayer H. 1986. Thermal comfort of man in different urban environments. *J. Theor. Appl. Climatol.* **38**: 43–49.
- Hurk van den B, Klein Tank A, Lenderink G, van Ulden A, van Oldenborgh GJ, Katsman C, van den Brink H, Keller F, Bessembinder J, Burgers G, Komen G, Hazeleger W, Drijfhout S. 2006. KNMI Climate Change Scenarios 2006 for The Netherlands. KNMI Scientific Report WR 2006-01, pp. 9–11, KNMI: De Bilt, The Netherlands.
- Huynen MMTE, Martens P, Schram D, Weijenberg MP, Kunst AE. 2001. The impact heat waves and cold spells on mortality rates in the Dutch population. *Environ. Health Perspect.* **109**: 463–470.
- Hwang RL, Lin TP, Matzarakis A. 2011. Seasonal effect of urban street shading on long-term outdoor thermal comfort. *Build. Environ.* **4**: 863–870.
- Johansson L. 2012. *Modeling near Ground Wind Speed in Urban Environments Using High Resolution Digital Surface Models and Statistical Methods: INES nr. 234*. Department of Physical Geography and Ecosystems Science Lund University, Lund, Sweden. Online available at <http://lup.lub.lu.se/luur/download?func=downloadFile&recordId=2534839&fileId=2534861>.
- Jones RG, Murphy JM, Hassell D, Taylor R. 2001. Ensemble mean changes in a simulation of the European climate 2071–2100 using the new Hadley Centre regional modelling system HadAM3H/HadRM3H. *Technical report*, Hadley Centre, Bracknell, UK
- de Jong E, van Boxel JH. 2012. Een analyse van het windklimaat in Nederland, University of Amsterdam, Amsterdam, The Netherlands, 32 pp (in Dutch). <http://dare.uva.nl/cgi/arno/show.cgi?fid=455625> (accessed 1 May 2013).
- Junk J, Matzarakis A, Ferrone A, Krein A. 2014. Evidence of past and future changes in health-related meteorological variables across Luxembourg. *Air Qual. Atmos. Health* **7**: 71–81.
- KNMI. 2005. *Handboek Waarnemingen*, Chapter 15 – Wolken (in Dutch). www.knmi.nl/samenw/hawa/pdf/Handboek_H15.pdf (accessed 30 April 2013)
- KNMI. 2012. *Hourly and daily data for the KNMI weather stations*. www.knmi.nl/klimatologie/uurgegevens/#no and www.knmi.nl/klimatologie/daggegevens/download.html (accessed 30 April 2013).
- KNMI. 2014. *KNMI'14-klimaatscenario's voor Nederland; Leidraad voor professionals in klimaatadaptatie*. KNMI: De Bilt, The Netherlands, 34 pp (in Dutch).
- Koopmans S, Theeuwes NE, Steeneveld GJ, Holtslag AAM. 2015. Modelling the influence of urbanization on the 20th century temperature record of weather station De Bilt (The Netherlands). *Int. J. Climatol.* **35**: 1732–1748, doi: 10.1002/joc.4087.
- Kusaka H, Kimura F. 2004. Thermal effects of urban canyon structure on the nocturnal heat island: numerical experiment using a mesoscale model coupled with an urban canopy model. *J. Appl. Meteorol.* **43**: 1899–1910.
- Lenderink G, van Ulden A, van den Hurk B, Keller F. 2007. A study on combining global and regional climate model results for generating climate scenarios of temperature and precipitation for The Netherlands. *Clim. Dyn.* **29**: 157–176.
- Lokys HL, Junk J, Krein A. 2015. Future changes in human-biometeorological index classes in three regions of Luxembourg, Western-Central Europe. *Adv. Meteorol.*, doi: 10.1155/2015/323856. <http://www.hindawi.com/journals/amete/2015/323856/>.
- Luber G, McGeehin M. 2008. Climate change and extreme heat events. *Am. J. Prev. Med.* **35**: 429–435.
- Matzarakis A, Amelung B. 2008. Physiologically Equivalent Temperature as indicator for impacts of climate change on thermal comfort of humans. In: M. C. Thomson, R. Garcia-Herrera, M. Beniston (eds.), *Seasonal Forecasts, Climatic Change and Human Health*. Advances in Global Change Research 30, Springer-Sciences and Business Media, 161–172.
- Matzarakis A, Mayer H. 1996. Another Kind of Environmental Stress: Thermal Stress. WHO Collaborating Centre for Air Quality Management and Air Pollution Control. *NEWSLETTERS* **18**: 7–10.
- Matzarakis A, Mayer H, Iziomon MG. 1999. Applications of a universal thermal index: physiological equivalent temperature. *Int. J. Biometeorol.* **43**: 76–84.
- Matzarakis A, Mayer H, Rutz F. 2000. *RayMan Version 1.2*. Meteorological Institute, University of Freiburg: Freiburg, Germany.
- Matzarakis A, Rutz F, Mayer H. 2007. Modeling radiation fluxes in simple and complex environments application of the RayMan model. *Int. J. Biometeorol.* **51**: 323–340.
- Matzarakis A, Rammelberg J, Junk J. 2013. Assessment of thermal bioclimate and tourism climate potential for central Europe – the example of Luxembourg. *Theor. Appl. Clim.* **114**: 193–202.
- Mayer H, Höppe P. 1987. Thermal comfort of man in different urban environments. *Theor. Appl. Clim.* **38**: 43–49.
- McCarthy MP, Best MJ, Betts RA. 2010. Climate change in cities due to global warming and urban effects. *Geophys. Res. Lett.* **37**: L09705.
- Müller N, Kuttler W, Barlag A. 2014. Counteracting urban climate change: adaptation measures and their effect on thermal comfort. *Theor. Appl. Climatol.* **115**: 243–257.
- Nijmeijer H. 2000. De Randstad en de Rest. *Index* **8**: 22–23. <http://www.cbs.nl/NR/rdonlyres/379841D2-BA32-4753-8A02-00B7F676D5F6/0/index1092.pdf> (accessed 15 February 2015).
- Oke TR. 1981. Canyon geometry and the nocturnal urban heat island: comparison of scale model and field observations. *J. Climatol.* **2**: 237–254.
- Oke TR. 1982. The energetic basis of the urban heat island. *Q. J. R. Meteorol. Soc.* **455**: 1–24.
- Oke TR. 1988. Street design and urban canopy layer climate. *Energy Build.* **11**: 103–113.
- Oleson K. 2012. Contrasts between urban and rural climate in CCSM4 CMIP5 climate change scenarios. *J. Clim.* **25**: 1390–1412.
- Oleson KW, Bonan GB, Feddema J, Jackson T. 2011. An examination of urban heat island characteristics in a global climate model. *Int. J. Climatol.* **31**: 1848–1865.
- Oleson KW, Monaghan A, Wilhelmi O, Barlage M, Brunsell N, Feddema J, Hu J, Steinhoff DF. 2015. Interactions between urbanization, heat stress, and climate change. *Climatic Change* **129**: 525–541.
- Rosenzweig C, Solecki WD, Parshall L, Chopping M, Pope G, Goldberg R. 2005. Characterizing the urban heat island in current and future climates in New Jersey. *Glob. Environ. Change Part B* **6**: 51–62.
- Santiago JL, Martilli A, Martín F. 2007. CFD simulation of airflow over a regular array of cubes. Part I: three-dimensional simulation of the flow and validation with wind-tunnel measurements. *Bound.-Layer Meteorol.* **122**: 609–634.
- Sherwood SC, Huber M. 2010. An adaptability limit to climate change due to heat stress. *Proc. Natl. Acad. Sci. U.S.A.* **107**: 9552–9555.
- Sluijter R, Leenaers H, Camarasa M. 2011. *De Bosatlas van het klimaat*. Noordhoff uitgevers: Groningen, The Netherlands, 112 pp (in Dutch) 9789001120894.
- Steenefeld GJ, Koopmans S, Heusinkveld BG, van Hove LWA, Holtslag AAM. 2011. Quantifying urban heat island effects and human comfort for cities of variable size and urban morphology in The Netherlands. *J. Geophys. Res.* **116**: D20129.
- Stewart ID, Oke TR. 2012. Local climate zones for urban temperature studies. *Bull. Am. Meteorol. Soc.* **93**: 1879–1900.
- Taleghani M, Kleerekoper L, Tenpierik M, van den Dobbelsteen A. 2015. Outdoor thermal comfort within five different urban forms in The Netherlands. *Build. Environ.* **83**: 65–78.
- Teixeira J, Stevens B, Bretherton CS, Cederwall R, Klein SA, Lundquist JK, Doyle JD, Golaz JC, Holtslag AAM, Randall DA, Siebesma AP, Soares PMM. 2008. Parameterization of the atmospheric boundary layer: a view from just above the inversion. *Bull. Am. Meteorol. Soc.* **89**: 453–458.
- Theeuwes NE, Steeneveld GJ, Ronda RJ, Heusinkveld BG, van Hove LWA, Holtslag AAM. 2014. Seasonal dependence of the urban heat island on the street canyon aspect ratio. *Q. J. R. Meteorol. Soc.* **140**: 2197–2210.
- Thorsson S, Lindberg F, Björklund J, Holmer B, Rayner D. 2011. Potential changes in outdoor thermal comfort conditions in Gothenburg, Sweden due to climate change: the influence of urban geometry. *Int. J. Climatol.* **31**: 324–335.
- Uejio CK, Wilhelmi OV, Golden JS, Mills DM, Gulino SP, Samenow JP. 2011. Intra-urban societal vulnerability to extreme heat: the role of heat exposure and the built environment, socioeconomics, and neighborhood stability. *Health Place* **17**: 498–507.
- vanUlden AP, van Oldenborgh GJ. 2006. Large-scale atmospheric circulation biases and changes in global climate model simulation and their importance for climate change in Central Europe. *Atmos. Chem. Phys. Discuss.* **5**: 7415–7455.

- Wever N, Groen G. 2009. Improving potential wind for extreme wind statistics. KNMI Scientific Report WR 2009-02. KNMI: De Bilt, The Netherlands.
- Wieringa J, Rijkoort PJ. 1983. *Klimaat van Nederland 2: Windklimaat van Nederland*. Staatsuitgeverij's-Gravenhage: Den Haag, The Netherlands.
- Wilby RL. 2003. Past and projected trends in London's urban heat island. *Weather* **58**: 251–260.
- Willett KM, Sherwood S. 2012. Exceedance of heat index thresholds for 15 regions under a warming climate using the wet-bulb globe temperature. *Int. J. Climatol.* **32**: 161–177.
- Wolters D, Brandsma T. 2012. Estimating the urban heat island in residential areas in The Netherlands using observations by weather amateurs. *J. Appl. Meteorol. Climatol.* **51**: 711–721.